A General and Robust Approach for Defining and Solving Microkinetic Catalytic Systems

Gabriel S. Gusmão
Dept. of Chemical and Environmental Engineering, University of California, Riverside, Riverside, CA 92521

School of Chemical Engineering (FEQ), University of Campinas; Campinas (UNICAMP), Campinas, SP 13083-852 Brazil

Renewable Technologies, Braskem S.A., Campinas, SP 13086-530 Brazil

Phillip Christopher
Dept. of Chemical and Environmental Engineering, University of California, Riverside, Riverside, CA 92521

Program in Materials Science & Engineering, University of California, Riverside, Riverside, CA 92521

DOI 10.1002/aic.14627
Published online September 30, 2014 in Wiley Online Library (wileyonlinelibrary.com)

Recent approaches for the rational design of heterogeneous catalysts have relied on first-principles-based microkinetic modeling to efficiently screen large phase spaces of catalytic materials for optimal activity and selectivity. Microkinetic modeling allows the calculation of catalytic rate and selectivity under a given set of conditions without a priori assumptions of rate or selectivity controlling steps by simultaneously solving nonlinear algebraic equations comprising species mass balances bound by the pseudo steady-state approximation. We introduce a general approach to define and solve microkinetic systems that relies solely on its stoichiometric matrix and kinetic parameters of considered reaction steps. Our approach relies on linearization of the microkinetic system, enabling analytical calculation of system derivatives for use in quasi-Newton solution schemes that exhibit excellent robustness and efficiency with minimal dependence on initial conditions. © 2014 American Institute of Chemical Engineers *AIChE J*, 61: 188–199, 2015
Keywords: microkinetics, catalytic modeling, analytical, heterogeneous catalysts, density functional theory calculations

Introduction

The discovery of optimized heterogeneous catalysts has classically been executed through a "trial and error" approach where empirically driven intuition is utilized to guide the search for optimal catalytic materials. Recent years have seen the emergence of rational approaches toward heterogeneous catalyst design that rely, in a large part, on utilizing *ab initio* calculation methods, such as density functional theory (DFT), as a guiding light for the experimental testing of new catalysts. One approach that has been executed successfully many times to identify novel materials for heterogeneous catalytic processes involves: (1) utilizing DFT calculations to map out the energetics of many possible reaction pathways, (2) performing massively parallel microkinetic modeling on the complex reaction pathways to efficiently screen the compositional and geometric phase spaces of catalytic materials and identify optimum candidates and (3) synthesizing and testing identified candidates. This approach has been used to identify novel heterogeneous metallic catalysts for ethylene epoxidation, alkyne hydrogenation, hydrodesulphurization, methanol synthesis from CO_2 among many others.[1–10]

At the heart of this proven catalyst design approach is the use of microkinetic models to predict the catalytic activity and selectivity of libraries of potential materials in complex reactions (systems of many parallel and competing elementary step pathways) as a function of reaction operation conditions. The microkinetic analysis approach of calculating activity and selectivity in complex heterogeneous catalytic reaction pathways makes no *a priori* assumptions regarding rate-limiting steps; rather, it involves the simultaneous solution of a set of nonlinear algebraic mass balances associated with surface bound species involved in the catalytic cycle. The mass balances are solved for a given set of conditions (T, P's) under the assumption that in a snapshot picture of the system, the concentration of adsorbate species are constant with respect to time; this is referred to as the pseudo steady-state approximation (PSSA).[11–13] Initial reactant and product concentrations are predefined at each condition for the calculation of instantaneous reaction rates at an exact location in a plug flow reactor operating at steady state, or the reaction rate at a given moment in an inherently transient batch reactor. Activation barriers, E_a and frequency factors, A, associated with each elementary step are estimated via DFT calculations or through surface science approaches, such as microcalorimetry, thermal desorption spectroscopy,

Additional Supporting Information may be found in the online version of this article.

Correspondence concerning this article should be addressed to P. Christopher at Christopher@engr.ucr.edu.

and vibrational spectroscopy.[5,6,14–25] The results of solving the system of equations at a given condition are adsorbate coverage, reaction rate, and selectivity. Typically, environmental conditions and rate constants (*T, P's, k's*) are varied to develop insights into how the system evolves under different conditions and provide important information regarding rate and selectivity controlling steps, in addition to allowing comparisons of predicted rate or selectivity of various potential catalysts. The microscale insights gained through this approach have proven indispensable for understanding surface catalytic processes and the design of new catalysts.

Microkinetic analysis has been typically executed by listing a set of assumed elementary step reactions involved in the overall catalytic process, gathering a database of the kinetic parameters, combining the rate equations into adsorbate mass balances and an overall catalytic site balance. The total number of sites in the overall site balance is normalized to 1, where each site is either vacant or occupied by an adsorbate.[5,11,12,26] The system of nonlinear equations is then solved using iterative approaches, which commonly utilize numerical differentiation of mass balances as a function of adsorbate coverage to guide the system toward the solution from the PSSA. Typical methods utilized to solve the nonlinear algebraic systems of mass balances are the trust-region methods and ordinary differential equation (ODE) solvers designed to solve differential algebraic equations (DAE).[27,28] Of particular difficulty is that convergence to the solution is highly dependent on the initial guess of adsorbate coverages, which results in the requirement of excessive iteration with varying levels of convergence criteria and numerical methods to achieve a solution with reasonable accuracy, without falling into local minima. The difficulty associated with obtaining ultimate solutions increases with the number of hypothesized intermediates. In addition, the enormous range that adsorbate coverage can span when dealing with complicated systems over wide variations in temperature and pressure along with the inaccuracy associated with finite-difference estimation of derivatives typically used by nonlinear solvers can make the convergence process unstable and erratic. These issues make the screening of potential catalytic materials for activity and selectivity inherently difficult, regardless of the rapidly developing approaches to calculate or estimate elementary step energetics on arbitrary catalyst surfaces.[29–31]

In this contribution, we introduce a general and robust quasi-Newton (QN) approach to solve microkinetic systems that only requires the input of a matrix that defines the stoichiometry of each reactant in each elementary step, which is typically referred to as Stoichiometric matrix,[32,33] and a vector defining kinetic parameters (E_a and A). We show that the Stoichiometric matrix can be utilized to deduce adsorbate mass balances in an automated manner. Taylor series expansion of the adsorbate mass balances allows the calculation of an analytical *Jacobian* matrix (and *Hessians*), encompassing first-order (and second-order) partial derivatives of the mass balances, which enables a highly robust solution method exhibiting system convergence at high levels of accuracy with minimal dependence on the initial conditions. In the following, we utilize a simple microkinetic model as descriptive guide through the development of the approach and follow this with a demonstration of its robust and efficient behavior in comparison to conventional solvers based on the trust-region dogleg method and fourth and fifth-order Runge–Kutta ODE solver methods. This highly efficient and simple approach for obtaining solutions of microkinetic models should facilitate the computational screening and design of catalytic materials.

(a) $A_2 + 2* \rightleftharpoons 2A*$

(b) $A* + B \rightleftharpoons C*$

(c) $C* \rightleftharpoons C + *$

Scheme 1. Three-step catalytic mechanism.

Forward	Reverse
$r_1 = k_1 p_A \theta_*^2$	$r_2 = k_2 \theta_{A*}^2$
$r_3 = k_5 \theta_{A*} p_B$	$r_4 = k_6 \theta_{C*}$
$r_5 = k_7 \theta_{C*}$	$r_6 = k_8 p_C \theta_*$

Scheme 2. Reactions rate equations.

Methodology Development

In this section, we utilize a simple three-step microkinetic model to allow for visualization of the mathematical manipulations in our solution approach. The three-step model, shown in Scheme 1, involves dissociative adsorption of a diatomic molecule (a), an Eley-Rideal-type associative adsorption of a second species (b) and product desorption (c).

In the example, *A, B*, and *C* are chemical species, and * represents a catalytic active site (e.g., enzyme sites, metal particle surface, etc.). In this example, the reaction is assumed to occur between gas and solid (surface) phases. Elementary step rate equations associated with the mechanism in Scheme 1 are shown in Scheme 2 and independently written for each of the forward and reverse elementary steps. Here, p_j represents the partial pressure of gas species j and θ_{j*} represents the normalized surface coverage occupied by adsorbed species j.

In the typical approach to microkinetic modeling, the rate equations would be used to define mass balances for all adsorbates. For example, the balance on θ_{A*} (the coverage of A on the catalyst) is given by Eq. 1. The mass balance is the sum of all generation and consumption reactions associated with a given species. Following the PSSA, it is hypothesized that at a given set of environmental conditions, the coverage of all surface intermediates does not vary significantly, and thus, Eq. 1, (1) is assumed to equal zero. In addition to the adsorbed species mass balances, a normalized site balance is used to solve for the concentration of free sites (catalytically active sites with no adsorbed species). After all adsorbed species mass balances and the site balance are defined and kinetic parameters have been estimated, the nonlinear system of algebraic equations could be solved to obtain surface coverage of adsorbates and rates. As stated above, the solution of the nonlinear system of equations can be difficult to obtain with typically used algorithms due to a significant number of local minima and the high variability of adsorbate coverage that lead to inconsistent solutions

$$2r_1 - 2r_2 - r_2 + r_4 = \frac{d\theta_{A*}}{dt} \tag{1}$$

To develop a general approach for solving complex microkinetic systems, we start by defining all species in the system as S_j's rather than p_j's and θ_j's. The rate equations

for all elementary steps are assumed to be of the power-law form: $r_i = k_i S_x^{\alpha_x} S_y^{\alpha_y}$ The rate constant k_i is assumed to follow the Arrhenius relationship, $k_i = A_i \exp(-E_{a_i}/kT)$. S_x and S_y represent the species concentrations, and α_x and α_y are the reaction order of the respective species in reaction rate equation i. The microkinetic system is defined as having n species and m reactions. Mass balances can then be defined in terms of S_j's, as the summation of the stoichiometry, $v_{j,i}$ of S_j in reaction i, multiplied by the reaction rate r_i, for all steps, Eq. 2. Stoichiometry is defined such that generation steps have positive stoichiometry, consumption steps have negative stoichiometry and when a species is not involved in an elementary step it has zero stoichiometry. For instance, as for the mass balance on θ_{A*}, Eq. 1, (1) where in reaction 1, θ_{A*} is formed in a second-order process and, therefore, r_1 has a positive coefficient of 2. In Eq. 2 the change in species S_j as a function of time, dS_j/dt, is defined as δ_j. The vector δ has a length of n and consists of all δ_j, in identical vertical order to S, and is a vector of 0's in the limit of the PSSA

$$\left\{\sum_i v_{j,i} r_i\right\} = \left\{\frac{dS_j}{dt}\right\} = \{\delta_j\} \tag{2}$$

Rather than enumerating all mass balances individually, the microkinetic system can be represented by a matrix that expresses the stoichiometry of each species in each reaction and a vector defining the reaction rate constants for all reactions. The Stoichiometric matrix, M, is defined as having n rows, which are associated with each of the species, S_j, and m columns, which are related to each of the reactions, r_i. Forward and reverse reactions are separately represented in M, where formation and consumption reactions are described by positive and negative stoichiometries, respectively. Although forward and reverse reactions are separately included as columns in M, the stoichiometry of the products for each reaction are also included in the definition of each elementary reaction. The Stoichiometric matrix, M, associated with the three-step model reaction, is shown on the left-hand side of Eq. 3, (3), and more generally can be written as $M_{j,i} = v_{j,i}$. In the context of the three-step example, the matrix M is vertically associated to each specific reaction ($r_1, r_2 \ldots r_m, m=6$) and is horizontally related to species mass balances ($S_1, S_2 \ldots S_n, n=6$). The reactions have been ordered as shown in the three-step mechanism definition and the species S_1 to S_6 by the order in which they appear in the mechanism, see right side of Eq. 3.

As mentioned previously, utilization of the PSSA requires concentrations of reactants and products to be defined for their rates of change at the defined condition to be evaluated. We developed an automated approach for the identification of products and reactants mass balance in M (discussed below), based on reactions for each species being entered into M in the order: reactant adsorption, surface reactions, and product desorption. The order in which surface reactions are inputted into M, however, does not impact the success of our approach in solving microkinetic systems, and thus, the approach is well suited for solving parallel surface reaction networks. However, the automated identification approach requires that when a reaction is split into forward and reverse steps, like reaction (a) in Scheme 1 into r_1 and r_2 in Scheme 2, the coupled reverse and forward reactions must be input into M in consecutive columns.

To demonstrate how reactions are represented in M, we can examine the first column in Eq. 3, which is associated with r_1. Examination of the first column shows that in r_1 the stoichiometry for S_1 is -1 and S_2 is -2, which correlates to first and second-order consumption reactions, respectively. It is also seen that S_3 has a coefficient of 2, which is related to the second-order production rate of S_3 in r_1. Inspection of the remaining columns shows that for each reaction, the stoichiometry of the reactants and products are included as negative and positive numbers, respectively. Furthermore, the stoichiometry for each reaction required to create the mass balance for a given species is found in the row associated with that species. For example, the mass balance for θ_{A*} (S_3) is defined in the row for S_3. M provides a complete description of the stoichiometry of all species in all reactions encompassed in the microkinetic system

$$\begin{array}{c} \\ S_1 \rightarrow \\ S_2 \rightarrow \\ \boldsymbol{S_3} \rightarrow \\ S_4 \rightarrow \\ S_5 \rightarrow \\ S_6 \rightarrow \end{array} \begin{array}{c} \begin{array}{cccccc} r_1 & r_2 & r_3 & r_4 & r_5 & r_6 \\ \downarrow & \downarrow & \downarrow & \downarrow & \downarrow & \downarrow \end{array} \\ \begin{bmatrix} \mathbf{-1} & 1 & 0 & 0 & 0 & 0 \\ \mathbf{-2} & 2 & 0 & 0 & 0 & -1 \\ 2 & -2 & -1 & 1 & 0 & \mathbf{0} \\ 0 & 0 & -1 & 1 & 0 & 0 \\ 0 & 0 & 1 & -1 & -1 & 1 \\ 0 & 0 & 0 & 0 & 1 & -1 \end{bmatrix}_{n \times m} \\ M_{j,i} = v_{j,i} \end{array} \begin{Bmatrix} p_{A_2} \\ \theta_* \\ \theta_{A*} \\ p_B \\ \theta_{C*} \\ p_C \end{Bmatrix} \rightarrow \begin{Bmatrix} S_1 \\ S_2 \\ S_3 \\ S_4 \\ S_5 \\ S_6 \end{Bmatrix} \tag{3}$$

$\boldsymbol{S}$

We can now entirely define the microkinetic system by introducing a vector, r, which describes the reaction rate equations associated with all reactions, Eq. 4. The vector r is vertical, has a length of m and is defined as the cross product of a diagonal matrix of k vector components, diag(k), and a vector, Ψ. The vector k is vertical, of length m and composed of the Arrhenius reaction rate constants, such that $k_i = A_i \exp(-E_{a_i}/kT)$, for each reaction, Eq. 5. The vector Ψ, depicted in Eq. 6, consists of the concentrations and reaction orders for each reaction. S_x and S_y represent reactants involved in reaction i. The indices x and y cannot be directly correlated with the indices defined for the vector S using an obvious mapping, because each species can be involved in different reaction rate equation throughout the microkinetic

system. For instance, in the definition of Ψ, in Eq. 7, S_2 and S_6 are both involved in the last reaction. Any sequential definition of species, based the order of the reactions, would not correctly define S_2 in both the first and last reaction steps. It is shown later that x's and y's can be implicitly defined by M, and are used here simply to represent two arbitrary species. With these definitions, the microkinetic system can be stated as the cross product of M and r equaling a vertical vector, δ, Eq. 7

$$r = \mathrm{diag}(k) \times \Psi \tag{4}$$

$$\{k\} = \{A\} \cdot \left\{ \exp\left(-\frac{E_a}{RT} \right) \right\} \tag{5}$$

$$\{\Psi\} = \{S_x^{\alpha x} S_y^{\alpha y}\} \tag{6}$$

$$\{M\} \times \{r\} = \{\delta\} \tag{7}$$

As previously stated, the goal of this approach is to obtain a complete description of the microkinetic system only relying upon the Stoichiometric matrix, M and the reaction rate kinetic parameters defined in k. To accomplish this, Ψ must be defined from M. A sequence of Boolean and matrix-based algebraic operations, which allow for the translation of M and the vector S into the vector Ψ, was developed and is shown in Eq. 8. $\hat{\Psi}$ is a matrix with individual entries that define the reaction order of each species in each reaction. $\hat{\Psi}$ is used to define Ψ, as shown in a step by step derivation in the Supporting Information (S.2). As stated above, S is a vector of length n, containing $S_1 \rightarrow S_n$ and is defined by the size of M (the vertical dimension). I is the identity matrix of size $n \times n$. The algebraic operations for defining Ψ from M identify entries into M associated with consumption reactions, (by focusing on the negative values in M) define them based on the order of the reactions and transform the matrix into a vector. Only consumption reactions are considered, because reaction rates are written in terms of consumption reactions, see Scheme 2. After identifying how to create Ψ from M and S, the general microkinetic problem can be explicitly evaluated.

As it has been shown that Ψ can be built from M and S, the solution to the microkinetic system can be written as shown in Eq. 9. Ψ is a vector of potentially nonlinear terms, second or third order elementary processes (or higher order if nonelementary steps are considered) and is the source of nonlinearity in the solution of the microkinetic system. For microkinetic models built from elementary reaction steps, Ψ will only contain terms that encompass products of at most two species. Reactions involving more than two species are assumed rare to occur in elementary steps during heterogeneous catalytic reactions. In addition, along similar reasoning, it is assumed that a single reactant should never have higher than a second order dependence in an elementary step

$$\underbrace{\begin{Bmatrix} S_1 \\ S_2 \\ S_3 \\ S_4 \\ S_5 \\ S_6 \end{Bmatrix}}_{\boldsymbol{S}} \Rightarrow \begin{array}{c} \hat{\Psi} = \prod_{i=\min(M)}^{-1} \left([\boldsymbol{M} \le \boldsymbol{i}]^{\boldsymbol{T}} \times \left(\mathbf{diag}(\boldsymbol{S}) - \mathbf{I} \right) + [\mathbf{1}] \right) \\ \{\Psi_i\} = \prod_{j=1}^{\mathbf{n}} (\hat{\Psi}_{\mathbf{i,j}} \neq \mathbf{0}) \end{array} \Rightarrow \underbrace{\begin{Bmatrix} S_1 S_2^2 \\ S_3^2 \\ S_3 S_4 \\ S_5 \\ S_5 \\ S_2 S_6 \end{Bmatrix}}_{\boldsymbol{\Psi}} \tag{8}$$

$$\underbrace{\begin{bmatrix} -1 & 1 & 0 & 0 & 0 & 0 \\ -2 & 2 & 0 & 0 & 1 & -1 \\ 2 & -2 & -1 & 1 & 0 & 0 \\ 0 & 0 & -1 & 1 & 0 & 0 \\ 0 & 0 & 1 & -1 & -1 & 1 \\ 0 & 0 & 0 & 0 & 1 & -1 \end{bmatrix}}_{\boldsymbol{M}} \times \underbrace{\mathrm{diag}\begin{Bmatrix} k_1 \\ k_2 \\ k_3 \\ k_4 \\ k_5 \\ k_6 \end{Bmatrix}}_{\mathrm{diag}(k)} \times \underbrace{dt\begin{Bmatrix} S_1 S_2^2 \\ S_3^2 \\ S_3 S_4 \\ S_5 \\ S_5 \\ S_2 S_6 \end{Bmatrix}}_{\boldsymbol{\Psi}} = \underbrace{\frac{d}{dt}\begin{Bmatrix} S_1 \\ S_2 \\ S_3 \\ S_4 \\ S_5 \\ S_6 \end{Bmatrix}}_{\boldsymbol{\delta}} \tag{9}$$

To overcome difficulties associated with solving the nonlinear system using standard numerical approaches, Ψ can be expanded and linearized using a first order Taylor Series expansion (i.e., truncated at its first order term). Because the nonlinearity in the microkinetic system of elementary steps should contain at most second order functions, it is expected that analytical derivatives utilized in linearized forms of the equations will provide a reasonable estimate of the original function. From a Taylor Series expansion, nonlinear terms in Ψ can be approximately represented as first order functions with initial guesses and derivatives of the functions extrapolated from that point. This is achieved by truncating each series expansion of rows in Ψ at the first derivative term, Eq. 10. As in any series expansion, there is an error associated with reducing the complexity of the system dependences and truncating the series summation, defined as ϵ in Eq. 10. This error will be reduced through iterative solution approaches and thus is disregarded

$$\Psi = \begin{Bmatrix} \left(S_{x_1}^{\alpha_{x_1}} S_{y_1}^{\alpha_{y_1}} \right)_0 + \left(\alpha_{x_1} S_{x_1}^{\alpha_{x_1}-1} S_{y_1} \right)_0 \Delta S_{x_1} + \left(\alpha_{y_1} S_{y_1}^{\alpha_{y_1}-1} S_{x_1} \right)_0 \Delta S_{y_1} \\ \vdots \\ \left(S_{x_m}^{\alpha_{x_m}} S_{y_m}^{\alpha_{y_m}} \right)_0 + \left(\alpha_{x_m} S_{x_m}^{\alpha_{x_m}-1} S_{y_m} \right)_0 \Delta S_{x_m} + \left(\alpha_{y_m} S_{y_m}^{\alpha_{y_m}-1} S_{x_m} \right)_0 \Delta S_{y_m} \end{Bmatrix} + \begin{Bmatrix} \epsilon_1 \\ \vdots \\ \epsilon_m \end{Bmatrix} \tag{10}$$

The linearized form of Ψ can be represented more succinctly by noticing, from (10), that there must exist a matrix, J_Ψ, that transforms a vector of ΔS's to represent Ψ's first order derivatives, Eq. 11. In this form, J_Ψ, is the *Jacobian* of the microkinetic system with respect to S. A simple algebraic manipulation can be used to create J_Ψ from S, M, and Ψ as shown in Eq. 12. The details and derivation of this transformation are shown in the Supporting Information (S.3). The algebraic operations calculate the partial derivatives of polynomial type functions and order them according to the linearized version of Ψ, Eq. 10. Now that J_Ψ has been derived from known components, the linearized representation of Ψ for the three step mechanism example is shown in Eq. 13

$$\{\Psi\}_m \cong \begin{Bmatrix} S_{x_1}^{\alpha_{x_1}} S_{y_1}^{\alpha_{y_1}} \\ \vdots \\ S_{x_m}^{\alpha_{x_m}} S_{y_m}^{\alpha_{y_m}} \end{Bmatrix}_0 + [J_\Psi]_{n\times m}{}^{T} \times \begin{Bmatrix} \Delta S_1 \\ \Delta S_1 \\ \vdots \\ \Delta S_{n-1} \\ \Delta S_n \end{Bmatrix} \tag{11}$$

$$\boldsymbol{J_\Psi} = \mathbf{diag}(\boldsymbol{S})^{-1} \times [-\boldsymbol{M} \cdot [\boldsymbol{M} < \mathbf{0}]] \times \mathbf{diag}(\boldsymbol{\Psi}) \tag{12}$$

$$\underbrace{\begin{Bmatrix} S_1S_2^2 \\ S_3^2 \\ S_3S_4 \\ S_5 \\ S_5 \\ S_2S_6 \end{Bmatrix}}_{\boldsymbol{\Psi}} = \underbrace{\begin{Bmatrix} S_1S_2^2 \\ S_3^2 \\ S_3S_4 \\ S_5 \\ S_5 \\ S_2S_6 \end{Bmatrix}_0}_{\boldsymbol{\Psi}_0} + \underbrace{\begin{bmatrix} S_2^2 & 2S_1S_2 & 0 & 0 & 0 & 0 \\ 0 & 0 & 2S_3 & 0 & 0 & 0 \\ 0 & 0 & S_4 & S_3 & 0 & 0 \\ 0 & 0 & 0 & 0 & 0 & 0 \\ 0 & 0 & 0 & 0 & 0 & 0 \\ 0 & S_6 & 0 & 0 & 0 & S_2 \end{bmatrix}_0}_{\boldsymbol{J_\Psi^T}} \times \underbrace{\begin{Bmatrix} \Delta S_1 \\ \Delta S_2 \\ \Delta S_3 \\ \Delta S_4 \\ \Delta S_5 \\ \Delta S_6 \end{Bmatrix}}_{\boldsymbol{\Delta S}} \tag{13}$$

The linearized microkinetic system is now defined by Eqs. 9 and 13, only from the inputs M and k. To achieve a unique solution to this system, redundancies in M, δ, J_Ψ, and ΔS must be removed. Equations 9 and 13 contain mass balances of surface species, including free sites, reactants and products and thus are overspecified by the known reactant/product concentrations and the concentration of free sites, which is defined by the normalized overall site balance. Because the total number of sites is normalized to 1, the concentration of free sites can be calculated independently after each iterative solution of surface coverage and thus should be removed from M and δ. Redundancies associated with the reactants and products must be completely removed from Ψ (J_Ψ and ΔS) while the over specification of the concentration of free sites can be resolved by implicitly including the site balance. Redundancy removal in M and δ can be achieved by simply removing mass balances associated with reactants, products, and free sites. In the context of the example mechanism, upon simplification, M transforms from a 6×6 matrix, into a 2×6 matrix and δ from a vector of length 6 into 2, as shown in Eq. 14. In certain situations, such as a poisoning adsorbate or spectator species that have no terminating desorption or reaction pathway, species may resemble a reactant or product unless more specific species identification routines are implemented. Additionally, species that have more than one reaction coordinate may resemble adsorbates and automated identification of these becomes a difficult task. In these cases, we encourage explicit identification of which lines of the stoichiometric matrix refers to gas phase species mass balances as an input into the calculations. Alternatively, for simpler systems these redundancies can be removed without knowing or defining reactants, products, or free sites, through a heuristic approach that relies on the order by which reaction steps were defined in M.

As discussed above, M is vertically related to each reaction and horizontally related to each species. Reactions are ordered in the matrix, such that they follow the chronology of the reaction coordinate. For example, the forward reaction associated with each reactant adsorption step is inputted into the matrix one column prior to the reverse reaction that is associated with the desorption of the same reactant species. When a reactant is adsorbed onto the catalyst surface a negative value of -1 or -2 (depending on whether the adsorption is molecular or dissociative) will appear in M as the first non zero integer in the row associated with that species. The negative value occurs because the gas phase reactant species is being consumed to produce an adsorbed species. Immediately following this negative value, along the same row associated with the adsorbing reactant species, there will be a positive stoichiometry value associated with the desorption of the reactant species, or the reverse reaction of the adsorption step. This means that for simple microkinetic systems reactants can be identified in M as rows that contain at least one pair (horizontally sequential) of non zero stoichiometries, the first of which is always a negative value. For nonelementary processes involving higher order dependences, this generality still holds, although the magnitude of the values could be greater than two. Rows 1 and 4 in M, see Eq. 14, can be identified as reactant species as they are the only rows with pairs of values, each of which start with a negative stoichiometry.

Along a similar thought process, rows associated with species that are products can be identified as those that contain at least one pair of non zero stoichiometries, the first of which is always a positive value. Examination of M in Eq. 14 shows that only Species 6, the last row, follows this criterion and can thus be omitted from the solution as it is a product with a predefined concentration. The last species type that must be removed from the description is the concentration of free sites. The row associated with the free active sites mass balance can be identified as one that must be superposition (linear combination) of reactant adsorption and product desorption steps; therefore, it orthogonally contains the same values as the reactants and products. In our example case, Species 2 can be identified as containing adsorption and desorption steps and can therefore be removed from the microkinetic description. Once reactants, products, and free active sites mass balances are identified, the rows in M and δ associated with these species can be

removed as shown in Eq. 14. The terms that define the rate equations, diag(k) and Ψ, are left untouched in this process because we are removing redundancies associated with over specified mass balances, but still need all reaction rate definitions to describe the irreducible mass balances. Similar analysis upon the Stoichiometric matrix to eliminate linearly depended mass balances has been described by Fishtik and Datta[33]

$$\begin{array}{l}[\textbf{adsorption}]\\ [\textbf{free sites}]\\ [\text{surface}]\\ [\textbf{adsorption}]\\ [\text{surface}]\\ [\text{desorption}]\end{array}\begin{bmatrix}\mathbf{-1} & \mathbf{1} & 0 & 0 & 0 & 0\\ \mathbf{-2} & \mathbf{2} & 0 & 0 & \mathbf{1} & \mathbf{-1}\\ 2 & -2 & \mathbf{-1} & \mathbf{1} & 0 & 0\\ 0 & 0 & -1 & 1 & 0 & 0\\ 0 & 0 & 1 & -1 & -1 & 1\\ 0 & 0 & 0 & 0 & \mathbf{1} & \mathbf{-1}\end{bmatrix} \times \mathbf{diag}(\boldsymbol{k}) \times \boldsymbol{\Psi} = \frac{d}{dt}\begin{Bmatrix}S_1\\ S_2\\ S_3\\ S_4\\ S_5\\ S_6\end{Bmatrix} \tag{14}$$

$$\boldsymbol{M}\Downarrow \qquad\qquad \boldsymbol{\delta}\Downarrow$$

$$\begin{bmatrix}\mathbf{2} & \mathbf{-2} & \mathbf{-1} & \mathbf{1} & \mathbf{0} & \mathbf{0}\\ \mathbf{0} & \mathbf{0} & \mathbf{1} & \mathbf{-1} & \mathbf{-1} & \mathbf{1}\end{bmatrix} \qquad \frac{\boldsymbol{d}}{\boldsymbol{dt}}\begin{Bmatrix}\boldsymbol{S_3}\\ \boldsymbol{S_5}\end{Bmatrix}$$

Unnecessary redundancies must also be removed from the linearized description of Ψ. Through the heuristic analysis of M, species have been catagorized as reactants, products, surface species, and free sites. Using the known species types, J_Ψ and ΔS can be simplified to remove redundancies. Rows in J_Ψ and ΔS associated with reactants and products can be discarded. This leaves behind only reaction rate descriptions that are necessary for defining the mass balances of surface species. The overall normalized site balance, stating that the sum of all adsorbed species concentrations and the concentration of free sites equals one, can then be used to further reduce J_Ψ and ΔS, such that they are consistent with the dimension of M and δ, and implicitly include the site balance. This is achieved by knowing that the sum of ΔS_i associated with the surface species and free site concentrations must be equal to 0 and replacing the ΔS associated with the site balance (ΔS_3 in the example) with $-\sum \Delta S_i$, Eq. 15. The substitution is shown in Eq. 16. The rows associated with the free sites balance can then be subtracted from the remaining columns, and the line in ΔS associated with free sites can be removed. This process results in J_Ψ and ΔS, with all redundancies removed and implicitly including the site balance

$$\sum \theta = 1 \therefore \sum \Delta\theta = 0 \tag{15}$$

$$\boldsymbol{\Psi} = \boldsymbol{\Psi}_0 + \begin{bmatrix}S_2^2 & 2S_1S_2 & 0 & 0 & 0 & 0\\ 0 & 0 & 2S_3 & 0 & 0 & 0\\ 0 & 0 & S_4 & S_3 & 0 & 0\\ 0 & 0 & 0 & 0 & 0 & 0\\ 0 & 0 & 0 & 0 & 0 & 0\\ 0 & S_6 & 0 & 0 & 0 & S_2\end{bmatrix}_0 \times \begin{Bmatrix}\Delta S_1 = 0\\ \Delta S_2 = -\Delta S_3 - \Delta S_5\\ \Delta S_3\\ \Delta S_4 = 0\\ \Delta S_5\\ \Delta S_6 = 0\end{Bmatrix} \tag{16}$$

$$\boldsymbol{J_\Psi^T}\Downarrow \qquad\qquad \boldsymbol{\Delta S}\Downarrow$$

$$\begin{bmatrix}-2S_1S_2 & -2S_1S_2\\ 2S_3 & 0\\ S_4 & 0\\ 0 & 1\\ 0 & 1\\ -S_6 & -S_6\end{bmatrix} \qquad \begin{Bmatrix}\Delta S_3\\ \Delta S_5\end{Bmatrix}$$

At this point, all redundancies in Eqs. 9 and 13 have been removed. The reduced descriptions of (9) and (13) can then be combined, Eq. 17, and reorganized to solve for ΔS, Eq. 18. This linearized form of the microkinetic system can be used in a QN's approach to solve for the adsorbed species concentrations at a given set of conditions. Inspection of Eq. 18 shows that M and diag(k) are inputted functions and δ is a vector of 0's, as defined by PSSA. J_Ψ, the *Jacobian* matrix, and Ψ_0, a vector of the initial reaction rates concentration dependent terms, were both phenomenologically derived and are initially defined by the initial guess of adsorbate coverages. The iterative solution algorithm can then be defined in Eq. 19, where the analytical *Jacobian* of the linearized microkinetic system guides the iterative process

$$[M \times \text{diag}(k)] \times \{\{\Psi_0\} + [J_\Psi]^T \times \{\Delta S\}\} = \{\delta\} \tag{17}$$

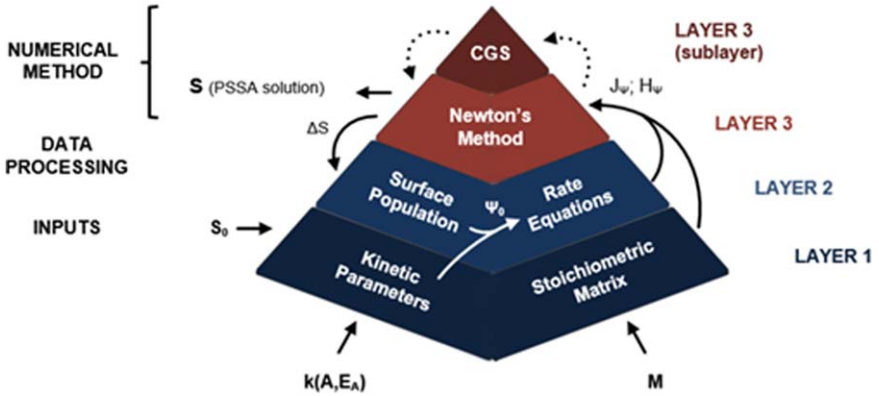

Figure 1. Structure of the microkinetic solution algorithm.

At the Layer 1 of the approach the stoichiometric matrix, M, the kinetic parameters, A and E_a, and adsorbate coverage initial guess S_0 are inputted. M is used to define Ψ, which is then used to define the systems derivatives J_Ψ and H_Ψ in Layer 2. In Layer 3, M, Ψ, J_Ψ, H_Ψ, and S_0 are used in the QN methods. Because the required matrix inversions in our approach can approach singularities, the conjugate gradient squares method is used to iteratively solve for ΔS when needed in a subroutine of Layer 3. This cycle is repeated until all adsorbate coverages reach convergence. [Color figure can be viewed in the online issue, which is available at wileyonlinelibrary.com.]

$$\{\Delta S\}=[M\times\mathrm{diag}(k)\times J_\Psi^T]^{-1}\times\{\{\delta\}-M\times\mathrm{diag}(k)\times\{\Psi_0\}\} \tag{18}$$

Equation 18 is utilized to calculate $\{\Delta S\}$ from the initial guesses of S (S_i) and provide a new S (S_{i+1}), using Eq. 19, thus minimizing the residues through a QN solution method. The new S can then be used to recalculate J_Ψ and Ψ_0, which sets up an iterative solution approach through the use of a convergence criterion for minimizing $\{\Delta S\}$. Throughout the remainder of the text, we will refer to this solution approach as a QN scheme and will specify the method used to calculate the system derivatives, that is, QN analytical *Jacobian*

$$\begin{aligned}&\{S\}_{i+1}=\{S\}_i+\{\Delta S\}_i\\&\text{until } \Delta S_i \text{ and } \delta_i < \text{ Convergence Criteria}\end{aligned} \tag{19}$$

We have also developed an analogous second order approach for solving microkinetic systems as an extension to the linear approach presented above, the details are given in the Supporting Information (S.3-5). The approach focuses on defining a *Hessian* matrix ($H\Psi$), second order derivatives, that is analytically evaluated as a function of the *Jacobian* (J_Ψ), surface coverage (S), and reaction rates ($\mathrm{diag}(k)\times\Psi$). To incorporate the *Hessian* into the solution approach, a two step QN method was developed that makes use of the *Hessian* matrix in an iterative subroutine within each convergence cycle to correct for error in ΔS estimation in Eq. 18 by the *Jacobian*. The analytical expression defining the *Hessian* calculation, redundancy reduction in the *Hessian* and the two step QN approach to solve the microkinetic system are all described in the Supporting Information (S.3-5). We will refer to this method as the QN analytical *Hessian* method. In addition to the two QN solution schemes described above, the analytical *Jacobian* and *Hessian* can be used in a variety of other solution methods, for example, a trust region method or explicit ODE integrators, such as the Runge–Kutta method, as we will show later.

It is also worth discussing numerical difficulties that may arise during the proposed solution algorithm and approaches to handle the issues. As shown in Eq. 18, the solution for ΔS relies on inverting the matrix product $M\times\mathrm{diag}(k)\times J_\Psi^T$. $M\times\mathrm{diag}(k)$ is a matrix with mainly zeroes and kinetic constants, which may vary by many orders of magnitude (e.g., from 10^3 to 10^{20}). In addition, the larger the system of microkinetic equations, the more computationally demanding it becomes to solve the system by inversion of the square and nonsymmetric matrix product $M\times\mathrm{diag}(k)\times J_\Psi^T$, as the resulting matrix may at some point appear numerically singular during the iterative process. There are several methods that are used to solve such linear systems, direct: decomposition, preconditioning, pivoting, scaling; or iterative: general minimum residue, conjugated gradients, among others. We utilized a combination of iterative and direct methods to solve Eq. 18. All matrix inversions in this work were first calculated utilizing MATLAB's built in matrix inversion scheme. However, when the inverted matrix was close to singular, the iterative nonstationary conjugate gradients squared (CGS) method[34] was used to calculate matrix inversions. We have included specific details on the solution method (CGS) and technical discussion on numerical issues in the Supporting Information (S.6). It is also important to stress that species with close to zero or below machine precision concentrations may cause issue in the partial derivative calculations. Therefore, before calculating *Jacobian* and *Hessian* matrices a sufficiently small number (ε_0) should be assigned to components in S that are equal zero. Roundoff errors might arise from this necessary modification depending on how small ε_0 is compared to the convergence criteria and this should be optimized.

The overall solution approach for the microkinetic systems used in this work is schematically depicted in Figure 1.

Results and Discussion

To demonstrate the use of our approaches for solving complex microkinetic systems, we replicated the results of many previously reported systems. Here, we focus on a microkinetic model for ethylene epoxidation previously developed by Stegelmann et al.,[19] but we stress that similar behavior was also observed for other tested systems. The model by Stegelmann et al. consists of 17 reactions (34 elementary steps when separating forward and reverse reactions), containing parallel surface reaction pathways and two steps which are nonelementary, containing functional

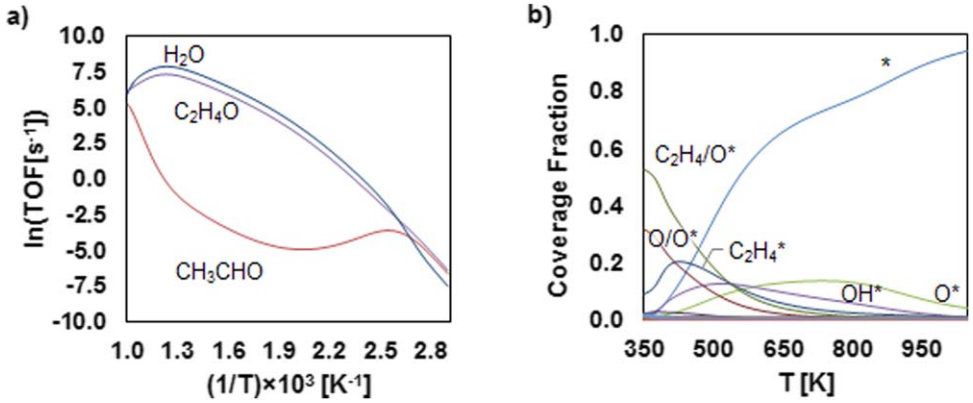

Figure 2. (a) Turn over frequency for the production of water, ethylene oxide (C_2H_4O), and acetaldehyde (CH_3CHO) as a function of inverse temperature and (b) surface coverage of various adsorbed species in the ethylene epoxidation microkinetic model as a function of operating temperature.

*** represents vacant catalyst sites while each surface species is denoted with * to identify it as a surface bound species. The results were calculated at with 0.5:0.5 C_2H_4:O_2 molar flow ratio at a total pressure of 2.0 atm. [Color figure can be viewed in the online issue, which is available at wileyonlinelibrary.com.]**

dependences higher than second order. This provides a test for the use of our approach to solve sufficiently complex networks including some nonidealities (nonelementary steps). In this model system, we assumed product concentrations of 0, meaning the results are initial rate calculations, equivalent to the initial time in a batch reactor or operating a continuous flow reactor at very low conversion. Figure 2a shows the turn over frequencies for water, ethylene oxide, and acetaldehyde production as a function of operating temperature, calculated using the approach described above; the QN analytical *Jacobian* method. In addition, Figure 2b shows the coverage of various adsorbates as a function of temperature. The magnitude and temperature dependence of the calculated turn over frequencies and adsorbate coverage are identical to those reported in the original paper. Agreement between results using our approach and other previously published results was also found, providing confidence that our approach identifies correct and reliable solutions to microkinetic systems.

To explore and distinguish the efficacy of our approaches, we broadly compare five methods in various stress tests and assess their numerical stability for the ethylene epoxidation microkinetic system. The five compared methods are: (1) the linearized QN approach relying on our analytical definition of the *Jacobian* at each iteration (QN analytical *Jacobian)*, (2) the linearized QN approach relying on central numerical differentiation of Ψ to obtain the *Jacobian* at each iteration (QN numerical *Jacobian*), (3) the trust region Dogleg method (built in code of MATLAB), with system derivatives defined by our analytical *Jacobian* at each iteration (TR Dogleg), (4) an ODE solver based on fourth and fifth order Runge–Kutta methods (built in code of the MATLAB Optimization Toolbox) having the *Jacobian* matrix calculated using our analytical definition at each iteration, and for each variable (ODE45) and (5) our two step QN approach relying on both the analytically defined *Jacobian* and *Hessian* at each iteration (QN analytical *Hessian*). Methods (1) and (2) are described above and Method (5) is described in the Supporting Information. Details regarding Methods (3) and (4) and our comparative testing approaches are described in more detail below.

Trust region methods are a family of numerical methods that have been broadly used and adapted in kinetic and reactor modeling to solve unconstrained systems of nonlinear equations[35–39]; furthermore, the TR Dogleg has been adopted by MATLAB as default nonlinear equation system solver.[27] The TR Dogleg method relies on a Newton's solution algorithm, similar to Eq. 19 above. In this work, we used our analytically defined *Jacobian* to calculate the system derivatives at each iteration step. In addition, the TR Dogleg method relies on the minimization of the square value of the first order linear representation of the microkinetic system to

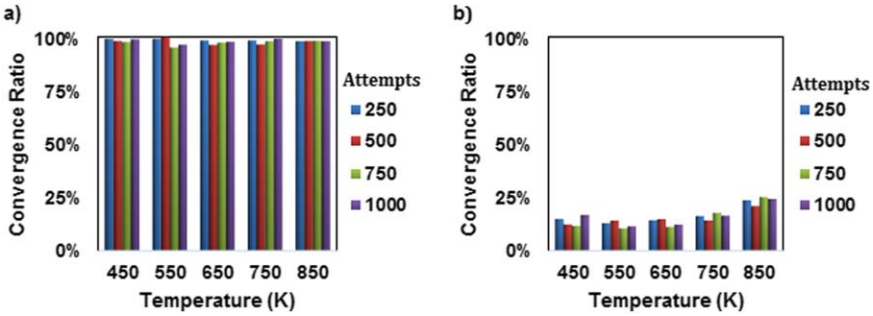

Figure 3. Convergence ratio (CR), defined as the percent of tested random initial conditions that converged to a solution, for the TR-Dogleg approach, (a), and QN analytical *Jacobian* method, (b), as a function of temperature for identical operating conditions as those used in Figure 2.

[Color figure can be viewed in the online issue, which is available at wileyonlinelibrary.com.]

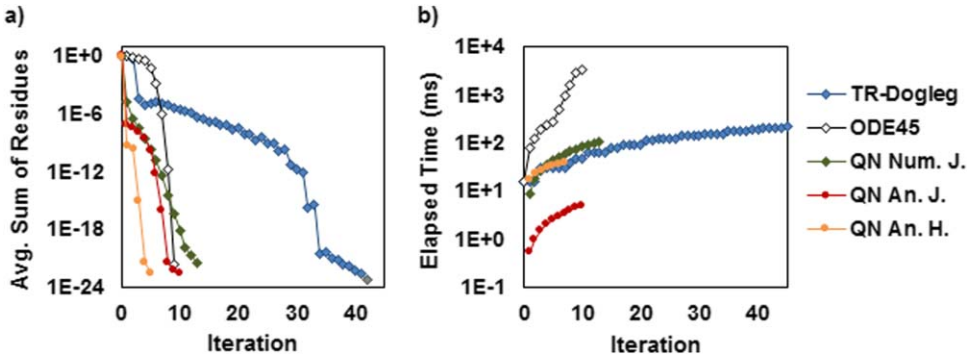

Figure 4. Average normalized sum of residuals ($\sum\delta_i$) for the tested approaches, (a), and average elapsed time (b), as a function of iteration number.

Results were obtained using an average of all converged solutions from the stress tests analyzed in Table 1. [Color figure can be viewed in the online issue, which is available at wileyonlinelibrary.com.]

define a local region over which the numerical differentiation may be "trusted."[40] To ensure the unbiased nature of the method comparisons, none of the TR Dogleg method's parameters were specified (i.e., maximum and minimum initial step length, maximum number of function evaluation, etc).

ODE methods (e.g., implicit, explicit or semi explicit methods), which are all highly dependent on consistent initial guesses[41], are also commonly applied onto DAE; for example, to solve microkinetic systems within the PSSA.[32] Our analytically defined *Jacobian* of the microkinetic system and approaches for redundancy removal provide a straightforward input matrix into typical approaches for solving systems of ODE's.[41] The removal of all degrees of freedom from the *Jacobian* and normalization of coverages to 1 minimizes constraints on the system that could bring about stiff system behavior. For the ethylene epoxidation microkinetic system, stiff and nonstiff ODE solvers were tested with the only significant difference in performance being increased time required to converge solutions for stiff solvers, and thus, we chose a standard nonstiff ode solver for comparison to other methods. We used a standard explicit ODE solver (ODE45 function), which uses fourth and fifth order Runge–Kutta methods. Within the ODE45 method, integration was executed through a normalized logspace (100 points, from −10 to 0.5 with maximum integration step size of the difference between the space points) to damp the integration step as the method approached solution and prevent numerical instabilities. Relative tolerance between derivatives estimated from fourth and fifth order Runge–Kutta methods was set to 5%. As mentioned above, CGS was used for the calculation of increment updates over the integration range whenever the built in MATLAB matrix invertor identified the system as close to singular.

Comparison of the five solution methods involved successive stress tests at specific conditions (temperature, total pressure, and reactant partial pressures) for uniformly distributed random initial guesses of coverage (S) using a 64 bit Intel Core i7 2637M; (4 CPU's ~1.70GHz), 8.2 GB RAM running MATLAB R2012b. Function and solution convergence tolerance of 10^{-8} (ΔS and $\delta_i < 10^{-8}$) were used in all tests, at maximum number of iterations (NI) of 10^3. We noticed that for systems that do not reach convergence after 10^3 iterations, succeeding iterations normally lead to inconsistent solutions. At each condition, convergence was attempted 250, 500, 750, and 1000 times with random initial guesses of S, to ensure the measured converged ratio had reached a constant value. Five equally spaced temperatures were utilized in the test: two at the opposite extremes—low temperature, thus low activity and high coverage, and high temperature, high activity, and low coverage—one at the mid range temperature and other two symmetrically distributed within the extremes and mid temperatures.

As an example of the type of results generated through this stress testing, Figure 3 displays the convergence ratio (CR, % of initial conditions attempted that reached a converged solution) for Method (1), QN analytical *Jacobian*, and Method (3), the TR Dogleg approach relying on the analytical *Jacobian*, over a range of temperatures, 450–850 K. In all cases, CR is constant for all attempt sample sizes, showing the sample size of random initial conditions of 250 is sufficient to represent a system average. For the QN analytical *Jacobian* approach, the CR is between 97–99% at all temperatures, showing robust behavior. Alternatively, the TR Dogleg approach utilizing the analytical *Jacobian*, exhibited a CR of approximately 15% at the lowest temperature and approximately 25% at the highest tested temperature. In addition to CR, for all tests where a solution converged we tracked the time to convergence (TC) and the NI required to

Table 1. Average Convergence Properties of the Tested Solvers (1250 Tests 450 to 850K), for the 17-step Ethylene Epoxidation Microkinetic Model; Same Conditions as for Figure 2: General Convergence Criteria: δ and $\Delta S<10^{-8}$; CGS Criteria 1.65×10^{-24}, $\varepsilon_0 = 1.74\times10^{-18}$; *Hessian* Subroutine Convergence Criteria: $\Delta_2 S<10^{-8}$ and 13 Iterations

Average Properties	QN Analytical Jacobian	QN Numerical Jacobian	QN Analytical Hessian	TR-Dogleg	ODE45
CR	0.98 ± 0.02	0.98 ± 0.01	0.97 ± 0.02	0.16 ±0.02	0.93 ± 0.02
TC (ms)	5.0 ± 0.2	200 ± 84	55 ± 5	200 ± 7	3300 ± 230
NI	11 ± 1	16 ± 1	7± 1	44 ± 2	10 ± 0

reach convergence. The CR, TC, and NI were tabulated for all tests (250 stress tests for five temperatures) and the average of these values for each solution approach (1–5) is provided in Table 1. In addition, the average of the normalized sum of δ_i residuals (to allow comparison of all runs with different initial conditions) and elapsed time as a function of iteration number, for all converged solutions, are shown in Figure 4.

We start our discussion by comparing results achieved using the analytical (Method 1) and numerical (Method 2) *Jacobian* as inputs to the linearized QN approach. The results in Table 1 show that both approaches exhibited CR's of near unity (98%), evidencing that the general linearized QN solution scheme is robust for solving the microkinetic system, regardless of initial condition. The significant advantage of using our analytically defined *Jacobian*, as compared to the typically used finite difference method derived *Jacobian*, can be seen in the average TC and NI in Table 1. Comparing the average behavior of these two approaches for 1250 random initial conditions (250 initial conditions for five temperature), the analytically calculated *Jacobian* reduced NI by >30% (from 16 to 11) and TC by approximately 40 fold compared to the numerically calculated *Jacobian*. The reduction in NI can be rationalized by the more accurate representation of the system derivatives calculated through an analytical approach rather than numerical differentiation. Graphically, this can be observed in Figure 4a, where it is shown that, on average, the analytical *Jacobian* provides a "better" first iteration in the solution process and a sharper trajectory toward solution convergence, as compared to the analytical *Jacobian*. The massive 40 fold reduction in TC is caused by the reduced computational demand of the analytical *Jacobian* calculation as compared to the central finite difference approach. These results are direct evidence of the benefit of analytically calculating the system *Jacobian*, rather than using more typical approaches of estimating the *Jacobian* based on finite difference methods.

Next, we compare the performance of Methods (1), (3), and (4), which all use the analytically calculated *Jacobian* within different solution frameworks: linearized QN (1), TR Dogleg (3) and ODE45 (4). The results in Table 1 show that the linearized QN approach exhibits the highest CR, 98%, compared to 16.5% and 93% for the TR Dogleg and ODE45 methods, respectively. This shows that when comparing the average behaviors of these solution approaches, while using an identical analytical method for calculating the system *Jacobian*, the linearized QN method is the most robust. A significant benefit of the linearized QN approach is observed in the TC, where the linearized QN exhibits a 40 fold and 660 fold reduction in TC compared to the TR Dogleg and ODE45 methods, respectively. As can been seen in Figure 4a, on average of all tested initial conditions the TR Dogleg approach exhibits a flat trajectory toward solution. This is due to the small magnitude of the "trusted region," causing the algorithm to exhibit sluggish and, due to high dependence on initial guesses, nonrobust solution behavior. These comparisons clearly show that the linearized QN approach is more effective than the TR Dogleg and ODE 45 solution methods, which also rely on the analytically calculated system *Jacobian*, in terms of robustness (CR) and efficiency (TC).

Finally, we compare the efficacy and robustness of our proposed two step QN *Hessian* method, based on the analytical *Hessian* and *Jacobian*, to all other tested methods. The QN *Hessian* approach exhibited a quantitatively similar CR as compared to the other QN approaches, showing robust behavior. In addition, the QN *Hessian* approach was the most efficient in terms of NI to reach convergence. In Figure 4a, this is seen as the steepest trajectory in residual minimization toward solution. The average TC (Table 1) was longer than for the QN analytical *Jacobian* approach, owing to the computational demand of the *Hessian* subroutine, but was shorter than that required for all other tested methods. Worth noting is that the average TC for the QN analytical *Hessian* also increases due to the fact that the microkinetic system being analyzed has higher than second order dependence in some of reaction rate equations. Otherwise, *Hessian* matrices calculation would only have to be done once as it becomes a constant matrix for DAE's of second order.

Analysis of the stress testing allows us to draw three conclusions regarding the efficacy of the compared approaches: (1) The use of our analytically defined *Jacobian*, as compared to numerical finite difference derived *Jacobian* within an identical solution scheme, provides a more efficient solution approach for the tested microkinetic system in terms of TC and NI, (2) the linearized QN scheme proved to be a more robust (CR) and efficient (TC) solution scheme compared to the TR Dogleg and ODE45 approaches, and (3) the inclusion of a second order subroutine, utilizing the analytical *Hessian*, in our proposed QN scheme allowed for a steeper solution trajectory in terms of residuals minimization and NI. It is also worth mentioning that we have developed a reflective subroutine for the QN approaches, which identifies when solutions are diverging toward an adsorbate poisoning condition (1 adsorbate has a coverage of 1 and all others 0), allowing for 100% CR in the ethylene epoxidation microkinetic system for all tested QN methods (analytical *Jacobian*, numerical *Jacobian* and *Hessian)*, see Supporting Information S6.

The ethylene oxidation microkinetic model showcased here includes mostly elementary steps; however, it also includes steps that aggregate higher order power law kinetic elementary processes with the highest reaction orders of 6. Even with this significant nonlinearity in two of the 17 reactions (34 elementary steps) in the model, our linearized solution approach provided a robust solution method over a wide range of operating conditions. In addition, the linearized system is capable of handling even the highly nonlinear behavior present between 375 and 475 K, where there is a shift in the species occupation trend, and the coverage of ethylene starts to diminish. Figure 2 shows the impact of the coverage change as an abrupt change in the Arrhenius Plot curves at 1/T around $2.5 \cdot 10^{-3}$ K^{-1}.

It is worth mentioning that although we have focused here on microkinetic systems with assumed constant adsorption energies and activation barriers as a function of species coverage, and kinetically controlled reaction rates, additional complexities can be included in this scheme and solved simultaneously within the core algorithm with the appropriate adaptations. Based on the high CR's and efficient convergence, even for nonelementary step nonlinearity in the microkinetic system, our approach represents a general and highly robust construct for analyzing catalytic systems that follow power law kinetics (heterogeneous, homogeneous and enzymatic), while only requiring the input of the Stoichiometric matrix, M and a vector containing the kinetic parameters of each reaction step.

Conclusion

In conclusion, we show a simple, robust and efficient approach for defining and solving microkinetic systems. The approach requires only the input of a matrix defining the stoichiometry of the elementary steps in the microkinetic system and a vector with the kinetic parameters of each elementary step. The Stoichiometric matrix can be reduced to form an irreducible representation of adsorbed species mass balances, which can be expanded using a Taylor's series, allowing the definition of an analytical *Jacobian* (as well as *Hessian*) describing variations in the microkinetic system. It was shown that the analytical calculation of system *Jacobians* facilitated higher efficiency (shorter NI and TC), as compared to numerically estimation of *Jacobians*, for solving microkinetic systems in our proposed QN solution scheme. By comparing the analytical *Jacobian* within solution schemes based on our QN approach, the TR Dogleg approach and a fourth and fifth order Runge–Kutta based ODE solver, our QN approach exhibited the highest convergence ratio, with the lowest required NI and time to solution. Finally, our proposed second order QN scheme based on the analytically defined *Jacobian* and *Hessian* displayed the most effective performance in terms of NI to reach convergence of all tested methods. Based on simplicity and flexibility, we expect our general linearized QN approaches to be particularly useful when there is a need of performing microkinetic modeling systematically for many catalytic systems to draw generalizable conclusions or for computational identification of optimum catalytic materials.[42]

Acknowledgment

P.C. acknowledges support from University of California, Riverside. G.S.G. acknowledges the Brazilian federal agency CAPES (the Brazilian Federal Agency for the Support and Evaluation of Graduate Education), through the Brazil Scientific Mobility Program, also referred to as Brazil Science Without Borders.

Literature Cited

1. Gundersen K, Jacobsen KW, Nørskov JK, Hammer B. The energetics and dynamics of H2 dissociation on Al(110). *Surf Sci.* 1994; 304:131–144.
2. Vlachos DG. Multiscale modeling for emergent behavior, complexity, and combinatorial explosion. *AIChE J.* 2012;58:1314–1325.
3. Greeley J, Nørskov JK, Kibler LA, El Aziz AM, Kolb DM. Hydrogen evolution over bimetallic systems: understanding the trends. *Chemphyschem* 2006;7:1032–1035.
4. Dumesic JA, Treviño AA. Kinetic simulation of ammonia synthesis catalysis. *J Catal.* 1989;116:119–129.
5. Salciccioli M, Stamatakis M, Caratzoulas S, Vlachos DG. A review of multiscale modeling of metal catalyzed reactions: mechanism development for complexity and emergent behavior. *Chem Eng Sci.* 2011;66:4319–4355.
6. Nørskov JK, Bligaard T, Rossmeisl J, Christensen CH. Towards the computational design of solid catalysts. *Nat Chem.* 2009;1:37–46.
7. Sehested J, Larsen KE, Kustov AL, Frey AM, Johannessen T, Bligaard T. Discovery of technical methanation catalysts based on computational screening. *Top Catal.* 2007;45:9–13.
8. Studt F, Abild Pedersena F, Wuc Q, Jensenc AD, Temeld B, Grunwaldte J D, Nørskova JK. CO hydrogenation to methanol on Cu–Ni catalysts: Theory and experiment. *J Catal.* 2012;293:51–60.
9. Mavrikakis M, Stoltze P, Nørskov JK. Making gold less noble. *Catal Lett.* 2000;64:101–106.
10. Lausche AC, Medfordb AJ, Khana TS, Xua Y, Bligaarda T, Abild Pedersena F, Nørskova JK, Studta F. On the effect of coverage dependent adsorbate–adsorbate interactions for CO methanation on transition metal surfaces. *J Catal.* 2013;307:275–282.
11. Neurock M. The microkinetics of heterogeneous catalysis. In: Dumesic JA, Rudd DF, Aparicio LM, Rekoske JE, Treviño AA, editors. *ACS Professional Reference Book.* Washington, DC: American Chemical Society, 1993.
12. Dumesic JA. Analyses of reaction schemes using de donder relations. *J Catal.* 1999;185:496–505.
13. Dumesic JA, Trevino AA, Milligan BA, Greppi LA, Balse VR, Sarnowski KT, Beall CE, Kataoka T, Rudd DF. A kinetic modeling approach to the design of catalysts: formulation of a catalyst design advisory program. *Ind Eng Chem Res.* 1987;26:1399–1407.
14. Panagiotopoulou P, Kondarides DI, Verykios XE. Selective methanation of CO over supported noble metal catalysts: effects of the nature of the metallic phase on catalytic performance. *Appl Catal A Gen.* 2008;344:45–54.
15. Madon RJ, Bradenb D, Kandoib S, Nagela P, Mavrikakisb M, Dumesicb JA. Microkinetic analysis and mechanism of the water gas shift reaction over copper catalysts. *J Catal.* 2011;281:1–11.
16. Medford AJ, Vojvodic A, Studt F, Abild Pedersen F, Nørskov JK. Elementary steps of syngas reactions on Mo2C(001): adsorption thermochemistry and bond dissociation. *J Catal.* 2012;290:108–117.
17. Holewinski A, Xin H, Nikolla E, Linic S. Identifying optimal active sites for heterogeneous catalysis by metal alloys based on molecular descriptors and electronic structure engineering. *Curr Opin Chem Eng.* 2013;2:312–319.
18. Silbaugh TL, Karp EM, Campbell CT. Surface kinetics and energetics from single crystal adsorption calorimetry lineshape analysis: methyl from methyl iodide on Pt(111). *J Catal.* 2013;308:114–121.
19. Stegelmann C, Schiødt NC, Campbell CT, Stoltze P. Microkinetic modeling of ethylene oxidation over silver. *J Catal.* 2004;221:630–649.
20. Yoshihara J, Campbell CT. Chemisorption of formic acid and CO on Cu particles on the Zn terminated ZnO (0001) surface. *Surf Sci.* 1998;407:256–267.
21. Starr DE, Diaz SF, Musgrove JE, Ranney JT, Bald DJ, Nelen L, Ihm H, Campbell CT. Heat of adsorption of Cu and Pb on hydroxyl covered MgO(100). *Surf Sci.* 2002;515:13–20.
22. Gokhale AA, Kandoi S, Greeley JP, Mavrikakis M, Dumesic JA. Molecular level descriptions of surface chemistry in kinetic models using density functional theory. *Chem Eng Sci.* 2004;59:4679–4691.
23. Herron JA, Tonelli S, Mavrikakis M. Atomic and molecular adsorption on Ru(0001). *Surf Sci.* 2013;614:64–74.
24. Herron JA, Tonelli S, Mavrikakis M. Atomic and molecular adsorption on Pd(111). *Surf Sci.* 2012;606:1670–1679.
25. Studt F, Sharafutdinov I, Abild Pedersen F, Elkjær CF, Hummelshøj JS, Dahl S, Chorkendorff I, Nørskov JK. Discovery of a Ni Ga catalyst for carbon dioxide reduction to methanol. *Nat Chem.* 2014;6: 320–324.
26. Koehle M, Mhadeshwar A. Microkinetic modeling and analysis of ethanol partial oxidation and reforming reaction pathways on platinum at short contact times. *Chem Eng Sci.* 2012;78:209–225.
27. Optimization Toolbox™: User's Guide MATLAB R2014a. Natick, MA, USA: The MathWorks, 2014.
28. Barrett R, Berry M, Chan TF, Demmel J, Donato JM, Dongarra J, Eijkhout V, Romine C, der Vorst HV. Templates for the Solution of Linear Systems: Building Blocks for Iterative Methods. Philadephia, PA, USA: Society for Industrial and Applied Mathematics, 1994.
29. Nørskov JK, Bligaard T. The catalyst genome. *Angew Chem Int Ed Engl.* 2013;52:776–777.
30. Lausche AC, Hummelshøj JS, Abild Pedersen F, Studt F, Nørskov JK. Application of a new informatics tool in heterogeneous catalysis: analysis of methanol dehydrogenation on transition metal catalysts for the production of anhydrous formaldehyde. *J Catal.* 2012;291: 133–137.
31. Abild Pedersen F, Greeley J, Studt F, Rossmeisl J, Munter TR, Moses PG, Skúlason E, Bligaard T, Nørskov JK. Scaling properties of adsorption energies for hydrogen containing molecules on transition metal surfaces. *Phys Rev Lett.* 2007;99:016105.
32. Stoltze P. Microkinetic simulation of catalytic reactions irreversible step. *Prog Surf Sci.* 2000;65:65–150.
33. Fishtik I, Datta R. A UBI–QEP microkinetic model for the water–gas shift reaction on Cu(111). *Surf Sci.* 2002;512:229–254.
34. Nachtigal NM, Reddy SC, Trefethen LN. How fast are nonsymmetric matrix iterations? *Soc Ind Appl Math.* 1992;13:778–795.
35. Soria MA, Mateos Pedreroa C, Marínd P, Ordóñez S, Guerrero Ruizb A, Rodríguez Ramosa I. Kinetic analysis of the Ru/SiO2

catalyzed low temperature methane steam reforming. *Appl Catal A Gen*. 2012;413–414:366–374.
36. Seth D, Sarkar A, Ng FTT, Rempel GL. Selective hydrogenation of 1,3 butadiene in mixture with isobutene on a Pd/α alumina catalyst in a semi batch reactor. *Chem Eng Sci*. 2007;62:4544–4557.
37. Patel K, Sunol A. Modeling and simulation of methane steam reforming in a thermally coupled membrane reactor. *Int J Hydrogen Energy* 2007;32:2344–2358.
38. Muñoz Batista MJ, Kubacka A, Gómez Cerezo MN, Tudela D, Fernández García M. Sunlight driven toluene photo elimination using CeO2 TiO2 composite systems: a kinetic study. *Appl Catal B Environ*. 2013;140–141:626–635.
39. Koeken ACJ, van den Broeke LJP, Deelman B J, Keurentjes JTF. Full kinetic description of 1 octene hydroformylation in a supercritical medium. *J Mol Catal A Chem*. 2011;346:1–11.
40. Nocedal J, Wright SJ, Robinson SM. Numerical Optimization. New York, USA: Springer Science, 2006.
41. Shampine LF, Reichelt MW, Kierzenka JA. Solving Index 1 DAEs in MATLAB and Simulink *. *Soc Ind Appl Math*. 1999;41:538–552.
42. Mhadeshwar AB, Vlachos DG. Is the water–gas shift reaction on Pt simple? *Catal Today*. 2005:105:162–172.

Manuscript received June 18, 2014, and revision received Sep. 2, 2014.